Quim. Nova, Vol. 40, No. 8, 849-853, 2017 http://dx.doi.org/10.21577/0100-4042.20170062

Artigo

PREPARATION AND VISIBLE LIGHT RESPONSIVE PHOTOCATALYTIC ACTIVITY OF Fe_3O_4/Ni-Al-Ce LDH/Bi_2WO_6 COMPOSITES

Jiaqi Hao, Ting Qu, Qiufeng Wang and Zhenbo Zhao*
School of Chemistry and Life Science, Changchun University of Technology, Changchun, Jilin, 130012, China

Recebido em 11/08/2016; aceito em 17/04/2017; publicado na web em 13/06/2017

Novel Fe_3O_4/Ni-Al-Ce LDH/Bi_2WO_6 composites were prepared through a hydrothermal method and co-precipitation method. The morphologies and structures of the photocatalysts were characterized by XRD, Raman, TEM, UV-vis-DRS, BET surface area and VSM techniques. The photocatalytic performances of the photocatalysts were investigated by the decolorization of methyl orange (MO) under visible-light irradiation. The results showed that the Fe_3O_4/Ni-Al-Ce LDH/Bi_2WO_6 composites exhibited greater photocatalytic activities compared to pure Bi_2WO_6 and the Ni-Al-Ce LDH; the decolorization rate of MO was 87% within 60 min under visible-light irradiation. The decolorization efficiency of the composite material remained at 71% after 4 recycling runs, showing improved stability. Furthermore, the experimental results also showed that the photocatalytic reactions for the composites followed first-order reaction kinetics. Therefore, the Fe_3O_4/Ni-Al-Ce LDH/Bi_2WO_6 composites were photocatalysts with high efficiencies and stabilities for a photocatalytic reaction of an organic pollutant, and this study provides a new, effective method for the development of wastewater treatment.

Keywords: hydrothermal method; co-precipitation; Fe_3O_4/Ni-Al-Ce LDH/Bi_2WO_6 composites; photocatalytic.

INTRODUCTION

With the rapid development of industries, water pollution becomes an increasingly serious problem, and the development of methods to resolve this issue becomes an important task of research for chemists and material scientists.[1,2] As an advanced oxidation technology, visible-light-driven photocatalytic technology has received significant attention owing to promising possibilities in wastewater treatment applications.[3] In the past few decades, many metal oxide semiconductors have been used as ideal photocatalysts due to their suitable band structures and great visible-light responses, including TiO_2,[4] ZnO,[5] CuO[6] and others.[7,8] Among them, Bi-based oxides have been extensively studied because of their unique band structures, where their valence bands are hybridized by Bi 6s and O 2p levels.[9]

Recently, Bi_2WO_6 has drawn great attention owing to its good photocatalytic performance in decolorization of organic pollutants under visible-light irradiation.[10,11] However, the photocatalytic efficiency of this single catalyst is not enough to be utilized because of its low quantum yield and high recombination rate of photogenerated electron-hole pairs.[12] To solve these problems, many methods have been proposed, such as the coupling of two semiconductors,[13] metal loading,[14] and ion doping.[15] Recent studies have indicated that composite photocatalysts possess higher responses for photocatalytic reactions because they can effectively promote separation of photogenerated electron-hole pairs and prolong the lifetime of charge carriers.[16]

Layered double hydroxides (LDHs) have attracted extensive attention and have been well researched for catalytic, biomaterial and electrochemical applications due to their unique properties allowing for tunable metal species and ratios and interlayer spacings.[17-19] As typical inorganic layered multifunctional materials, the photocatalytic application of LDHs has also attracted interest of researchers. The unique layered structure not only can increase active sites by enlarging the specific surface area but can also suppress the recombination of photogenerated charge carriers when these materials are coupled to another semiconductor.[20] Rare-earth elements have been extensively adopted in various materials, including catalysts, luminescent materials and aerospace alloys, owing to their unique electronic configurations, especially cerium. Seftel *et al.* prepared self-organized CeO_2 nanoparticles on highly dispersed ZnO_6/SnO_6 octahedral units provided by a layered double hydroxide via a simple and environment friendly synthesis procedure. In addition, this research indicated that the novel photocatalyst has better photocatalytic performance.[21,22] Additionally, Fe_3O_4 composites have also been widely studied over the past few decades, for example in catalysis,[23] analytical chemistry,[24] and electrochemistry,[25] due to their magnetically recoverable and reusable characteristics.

In this work, we have prepared a ternary hydrotalcite material through the introduction of rare-earth ions with large ionic radii. In addition, the Fe_3O_4/Ni-Al-Ce LDH/Bi_2WO_6 composites were synthesized by a solvothermal method and co-precipitation method. The combination of Ni-Al-Ce LDH with Fe_3O_4 and Bi_2WO_6 not only improves the photocatalytic activity but also allows the catalyst to be recycled.

EXPERIMENT

Preparation of catalysts

Fe_3O_4 synthesis: $FeCl_3{\cdot}6H_2O$ (99%, S.C.R Co., Ltd) and $FeSO_4{\cdot}7H_2O$ (99%, S.C.R. Co., Ltd) were each dissolved in distilled water. The two solutions were mixed together under vigorous stirring in a water bath at 65 °C. Then, NaOH (96%, B.C. Works) was slowly added into the solution. After the addition of SDS (T.F.C. Reagents Factory), the mixture was stirred for 30 min and then sealed in a Teflon-lined stainless steel autoclave, which was heated to 200 °C and kept for 8 h. The resultant solid was sequentially washed several times with water and ethanol and dried at 60 °C.

Bi_2WO_6 synthesis: $Bi(NO_3)_3{\cdot}5H_2O$ (99%, X.C. Co. Ltd.) and $Na_2WO_4{\cdot}2H_2O$ (99.5%, T.K.T.D. Co., Ltd.) were separately dissolved in ethylene glycol (96%, B.C. Works). After the two solutions were

*e-mail: zhaozhenbo@ccut.edu.cn

mixed together, ethanol was slowly added into the solution, and the solution was stirred for 10 min. The resulting clear solution was transferred to a 100 mL Teflon-lined stainless steel autoclave and was heated at 170 °C for 12 h. The product was obtained after filtering the solution, washing and drying at 80 °C. The as-prepared sample was then annealed at 300 °C for 3 h and ground into a fine powder.

Fe_3O_4/Ni-Al-Ce LDH/Bi_2WO_6 composite synthesis: 0.3712 g of Fe_3O_4 was ultrasonically dispersed into distilled water. Then, 7.0, 3.5, and 1.8 g of Bi_2WO_6 were added, and the mixture was sonicated for 20 min to obtain a uniform suspension. Then, the suspension was transferred into a 500 mL flask with vigorous stirring. An alkaline solution (100 mL, Na_2CO_3 (99%, X.C. Co., Ltd.), NaOH (96%, B.C. Works)) was added dropwise into the suspension until a pH of ca. 10.0 was reached, and the suspension was kept for 5 min before 100 mL of both salt solution ($Ni(NO_3)_2{\cdot}6H_2O$ (99%, T.K.T.D. Co., Ltd.), $Ce(NO_3)_3 6H_2O$ (99%, T.K.T.D. Co., Ltd.), and $Al(NO_3)_3{\cdot}9H_2O$ (99%, T.K.T.D. Co., Ltd.)) and the above alkaline solution were simultaneously added, maintaining the pH at 9.5-10. The products were collected by filtration, washed three times with water and dried at 60 °C in an oven. The samples were named A1, A2, and A3. Fe_3O_4/Ni-Al-Ce LDH was also prepared via a similar process but without the addition of Bi_2WO_6.

Characterization

Powder X-ray diffraction (XRD) was carried out using a D/max-IIA model diffractometer with Cu Kα radiation (30 kV, 20 mA). UV-vis diffuse reflectance spectra were obtained on a Carry 5000 spectrophotometer with a $BaSO_4$ reference. The surface morphology of the composite was analyzed with transmission electron microscopy (JEM-2010EX, 100 kV, magnification 100000). The magnetic properties of the samples were measured in a vibrating sample magnetometer (Quantum Design Corporation). The specific surface areas and pore structures were probed by measuring volumetric N_2 adsorption-desorption isotherms at liquid-nitrogen temperature (ASAP 2020 HD88).

Photocatalytic testing

The photocatalytic ability of the catalyst was measured through the decolorization of methyl orange solution under visible-light irradiation. A 400 W metal halide lamp (OCRS-II, HXSEI) was used as the light source. The sample (0.4 g) was dispersed into a 400 mL; 10 mg L^{-1} methyl orange solution under magnetic stirring. Before light irradiation, the suspension was stirred in the dark for 1 h to reach the adsorption-desorption equilibrium. To obtain the photocatalytic activity, samples were taken every 15 min. The samples were analyzed by a UV-vis spectrophotometer (Carry 5000, Agilent Technologies). All the photocatalytic tests were carried out under the same conditions. To control the reaction temperature, we utilized cycle cooling equipment (DC-0506, Temperature range -5~100 °C, Shanghai Hengping instrument factory) and maintained the temperature at 20 °C. To evaluate the stability of the composites, recycling reactions were carried out for the decolorization of methyl orange for composite A2 under visible-light irradiation.

RESULTS AND DISCUSSION

The X-ray diffraction patterns of Bi_2WO_6, Fe_3O_4/Ni-Al-Ce LDH and a series of Fe_3O_4/Ni-Al-Ce LDH/Bi_2WO_6 composites are shown in Figure 1(a). The pure Bi_2WO_6 sample has four peaks, corresponding to the orthorhombic phase of Bi_2WO_6 (JCPDS No. 73-1126).[26,27] The peaks of the Ni-Al-Ce LDH sample are also similar to previous research.[28] From Figure 1(a), we also find that the major peaks of the composites (A1, A2 and A3) are in agreement with those of pure Bi_2WO_6. This is because the amounts of LDH in the composites are very small. However, as the LDH content is increased, the characteristic peaks of the LDH at 11.5° and 35° are observed. Therefore, this proves that the series of Fe_3O_4/Ni-Al-Ce LDH/Bi_2WO_6 composites were successfully synthesized. Figure 1(b) shows the Raman spectra of the synthesized samples. For pure Bi_2WO_6, the peaks at 600-1000 cm^{-1} can be assigned to the stretching vibration of W-O.[29] The band at 310 cm^{-1} can be assigned to translational modes involving the simultaneous motions of $Bi^{3+}$and WO_6^{6-}.[30] Additionally, the peaks at 700 and 790 cm^{-1} are interpreted as the antisymmetric bridging mode associated with the tungstate chain and the antisymmetric A_g mode of the terminal O-W-O groups, respectively.[31] Compared with pure Bi_2WO_6, the intensities of the peaks of the composites obviously changed. The intensities of the peaks at 850 and 310 cm^{-1} increased, which might be attributed to some of the atoms of the LDH being doped into the O-W-O lattice.[3] This result further testifies that the novel composite was synthesized successfully.

Figure 2(a) shows the UV-vis diffuse reflectance spectra of the samples. The absorption edge of Bi_2WO_6 is found at approximately 440 nm, which is in accordance with reported research.[13] The absorption edges of the composites are more shifted into the visible region compared with Bi_2WO_6. According to the relationship between

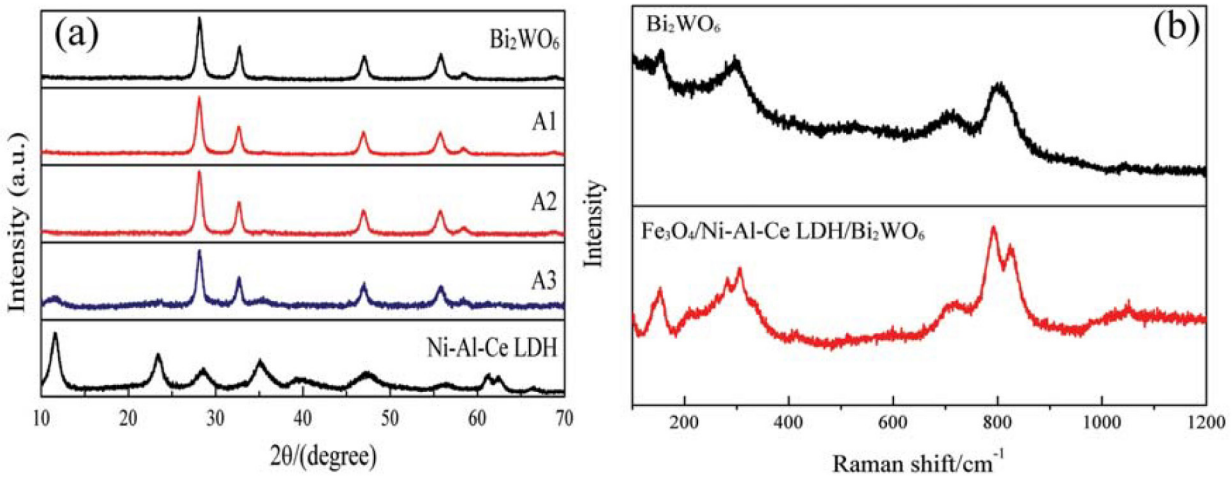

Figure 1. *(a) XRD patterns of the different samples; (b) Raman spectra of the samples*

$(\alpha h\nu)^2$ and quantum energy of light ($h\nu$),[32,33] we calculated the band gaps of the samples.

The band gaps of the different samples decreased in the following order: Fe_3O_4/Ni-Al-Ce LDH (2.62 eV) < A3 (2.64) < A2 (2.68) < A1 (2.71) < Bi_2WO_6 (2.86 eV). The presence of Fe_3O_4/Ni-Al-Ce LDH is beneficial for reducing the band gap of Fe_3O_4/Ni-Al-Ce LDH/Bi_2WO_6. The band gap narrowing of the composite is possibly attributed to the formation of a core-shell structure, which builds a new molecular orbital and narrows the band gap. According to the UV-vis results, we can make the reasonable assumption that the Fe_3O_4/Ni-Al-Ce LDH/Bi_2WO_6 composite could enhance the photocatalytic activity under visible-light irradiation. From Figure 2(b), we find that the samples have less coercivity and remanence, indicating that the catalysts have good superparamagnetism.[34] The magnetic saturation (1.2 emu g^{-1}) of A2 is lower than that of Fe_3O_4 (6.8 emu g^{-1}). The possible reasons for this are that the content of Fe_3O_4 in the composite is too little and that the surface of Fe_3O_4 is covered by Ni-Al-Ce LDH. From Figure 2(b), we can also find that the magnetic saturation of the recycled catalyst decreases, but it still possesses magnetism. Hence, we can draw a conclusion that a magnetic material is synthesized, and it is useful for recycling and reusing.

The morphologies and structures of Bi_2WO_6 and the Fe_3O_4/Ni-Al-Ce LDH/Bi_2WO_6 composite were observed by TEM, and the images are shown in Figure 3. From Figure 3(a), we see that the pure Bi_2WO_6 particles exhibit a distinct sheet structure. In addition, the morphology of the composite is shown in Figure 3(b) and 3(c). The core-shell structure of the composite was formed between the Bi_2WO_6 and Fe_3O_4 coating with the Ni-Al-Ce LDHs. This is benefit to the separation of photogenerated electrons and holes.

It is well known that the activity of a photocatalyst is strongly influenced by its surface properties.[35,36] The specific surface areas of pure Bi_2WO_6, the Fe_3O_4/Ni-Al-Ce LDH and a series of Fe_3O_4/Ni-Al-Ce LDH/Bi_2WO_6 nanoparticles were investigated by nitrogen adsorption-desorption isotherm analyses, and the results are listed in Table 1. The results reveal that the surface areas of pure Bi_2WO_6 and the Fe_3O_4/Ni-Al-Ce LDH are 22.29 and 236.07 m^2 g^{-1}, respectively. From Table 1, we can also see that the pore sizes of A1, A2 and A3 are 12.75, 3.96 and 2.83 nm, respectively. As the content of Bi_2WO_6 decreases, the surface area of the composite material increases. In addition, the pore size of sample decreases. The relatively larger specific surface areas of the Fe_3O_4/Ni-Al-Ce LDH/Bi_2WO_6 nanoparticles are useful for better adsorption of organic molecules and provide a greater number of reactive sites for the photocatalytic process, thereby, enhancing the photocatalytic performance.[22,37] However, the pore volume of A2 was larger than A3, and the possible reason for this is that the pore had collapsed when the structure of the composite material formed.

The photocatalytic activities of the samples were measured by the photocatalytic reaction of MO, and the results shown in Figure 4(a). Compared with pure Bi_2WO_6, the photocatalytic activities of the composite materials for MO exhibited large enhancements. This is attributed to the increased specific surface area as the content of

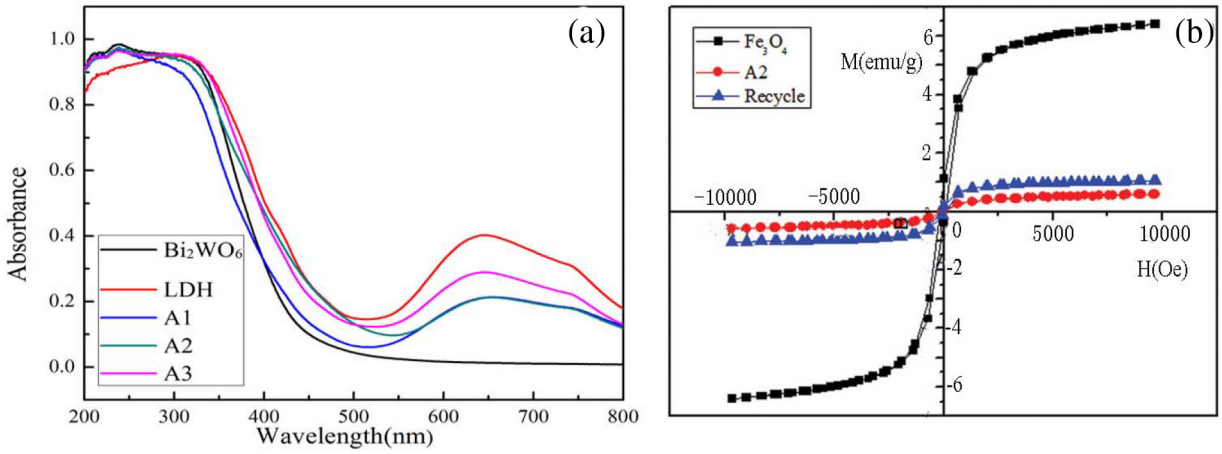

Figure 2. *(a) UV-vis diffuse reflectance spectra of the samples; (b) the magnetization curves of Fe_3O_4, A2 and the recycled catalyst*

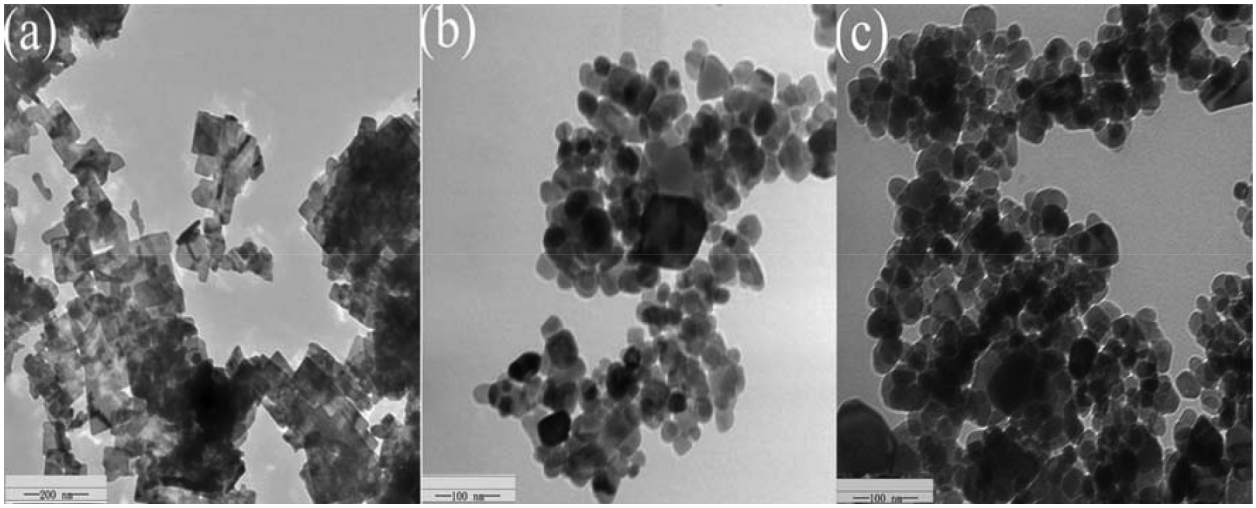

Figure 3. *TEM images of (a) Bi_2WO_6 and (b, c) the Fe_3O_4/Ni-Al-Ce LDH/Bi_2WO_6 composite (A2)*

Table 1. BET surface areas, pore volumes and pore sizes of the samples

Catalyst	BET surface area / $m^2\ g^{-1}$	V_{pore} / $cm^3\ g^{-1}$	d_{pore} / nm
Bi_2WO_6	22.29	0.19	33.41
LDH	236.07	0.36	5.89
A1	40.21	0.07	12.75
A2	151.85	0.15	3.96
A3	195.90	0.14	2.83

LDH increases, which can provide more active sites.[36] However, the photocatalytic activity reduced as the LDH content continued to increase. The possible reason for this is that the increased surface areas of the composites not only provide more active sites but also add recombination centers for the photogenerated electron-hole pairs. Under visible-light irradiation, the degradation rate of A2 was 87% within 60 min, which is higher than pure Bi_2WO_6 and the LDH. The possible reason for this is that the A2 composite material had an appropriate pore volume, which is beneficial for molecules accessing the internal surface of the catalyst. Thus, the efficiency of the catalytic reaction improved.

We also calculated the decolorization rate constants *k* for various samples, and the results are shown in Figure 4(b). The *k* values of the composite materials (A1, A2 and A3) are higher than pure Bi_2WO_6 and the LDH, and the A2 composite exhibited the maximum *k* value. This result indicates that A2 possesses higher photocatalytic activity. This may be attributed to the larger specific surface area and appropriate pore volume of the A2 composite, which provides more active sites. This result further illustrates that the composite materials possess preferable photocatalytic activities.

To evaluate the reusability of the prepared composite during the photocatalytic reaction, recycling experiments were carried out under visible-light irradiation. As shown in Figure 4(c), the composite shows better stability, and the decolorization efficiency of the composite material remained at 71% after the fourth recycling run. Because the synthesized composites possess magnetization, this is beneficial for recycling and reusing.

To explore the photocatalytic performance of the material, degradation experiments were carried out with different concentrations of MO. In addition, the first-order reaction rate equations are shown in Table 2, indicating that the photocatalytic process of MO decolorization conforms to first-order kinetics.[38,39] From Table 2, we find that the reaction rate constant decreased as the methyl orange concentration increased. As is well-know, physical interpretation of reaction rate constant is reaction rate of unit concentration (1 mol L^{-1}). Under visible light irradiation, photocatalyst was excited and produce photogenerated electron-hole pairs. Photogenerated electrons and holes can react with reactant directly or form stronger reactive species react with reactant, so as to achieve the purpose of the degradation of organic pollutants. Therefore, photocatalytic reaction rate depends on the amount of catalyst. When the concentration of reactant increased and the mass of the photocatalyst was constant, unit concentration corresponding to the amount of photocatalyst reduced. However, the mass of catalyst is critical for photocatalytic reaction rate. Hence, the reaction rate decreased and the rate constant decreased.

Table 2. Kinetic parameter of A2 composite (0.4 g) for photocatalytic decolorization of different concentration of MO

c_0 (mg L^{-1})	First-order reaction kinetics equation	R
10	$\ln(c_0/c) = 3.42\times10^{-2}\ t + 1.47\times10^{-1}$	0.98
12	$\ln(c_0/c) = 3.42\times10^{-2}\ t - 0.44\times10^{-2}$	0.99
14	$\ln(c_0/c) = 2.57\times10^{-2}\ t + 7.35\times10^{-2}$	0.98
16	$\ln(c_0/c) = 1.23\times10^{-2}\ t + 1.03\times10^{-2}$	0.99

To determine the main active species generated in the photocatalytic process, including superoxide radicals ($\bullet O_2^-$), hydroxyl radicals (•OH), electrons (e^-) and holes (h^+), trapping experiments were carried out under visible irradiation. Benzoquinone was used for quenching superoxide radicals.[40] Potassium dichromate and sodium oxalate were used as e^- and h^+ scavengers, respectively, and *tert*-butyl alcohol was used as a •OH scavenger.[41,42] Figure 5(a) displays the effects of different scavengers on the degradation of MO. We find that the catalytic abilities of the samples show no obvious changes with the addition of *t*-BuOH, indicating that •OH is not the main reactive species in the photocatalytic reaction. However, the catalytic abilities decreased obviously with added benzoquinone, potassium dichromate and sodium oxalate, and the influence of benzoquinone was the most significant. Based on the experiment results, we can draw a conclusion that $\bullet O_2^-$, e^- and h^+ are the main active species for the photocatalytic process.

Based on the above results, we suggest a possible photocatalytic reaction mechanism, which is explained in Figure 5(b). From the picture, we see that the CB position of Bi_2WO_6 is set at -0.43 eV is more negative than that of the LDH (0.73 eV). Therefore, the electrons in the CB of Bi_2WO_6 will transfer to the CB of the LDH.[43] In addition, the VB of the LDH (3.35 eV) is more positive than LDH, and the

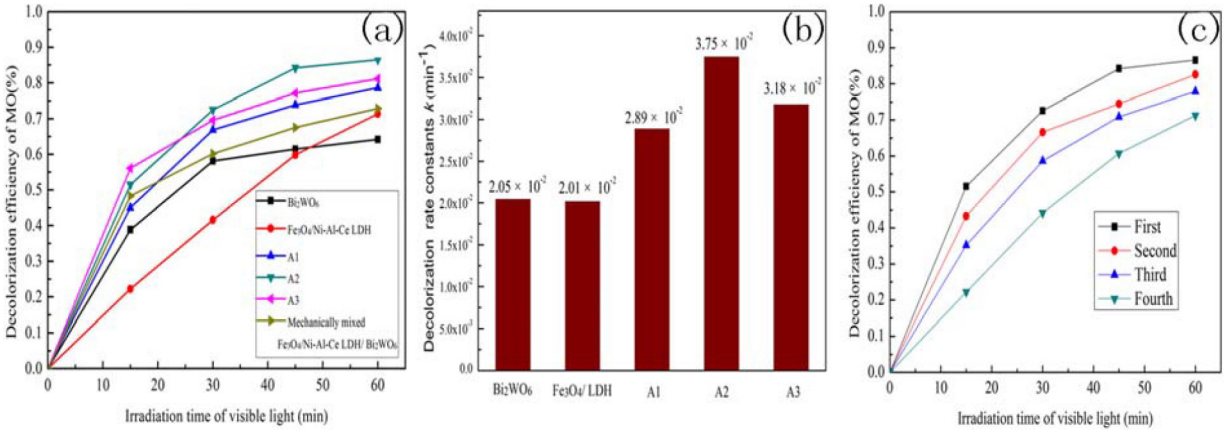

Figure 4. *(a) Photocatalytic decolorization of MO (10 mg·L^{-1}) for the various catalysts at 20 °C; (b) Photocatalytic decolorization rate constants k (min^{-1}) of the various samples; (c) Recycling runs for the photocatalytic decolorization of MO (10 mg·L^{-1}) with the A2 composite (0.4 g) at 20 °C*

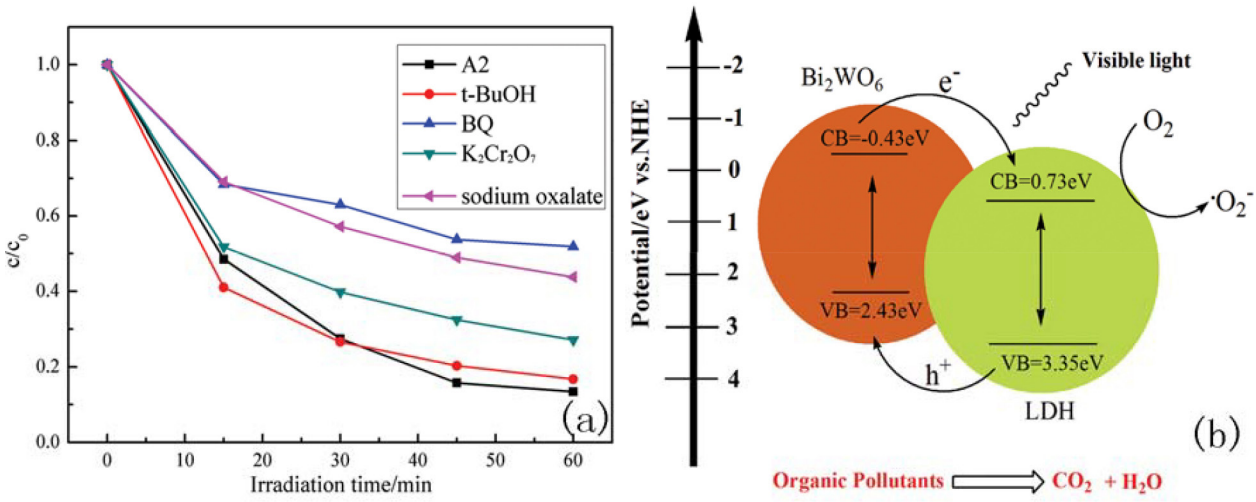

Figure 5. *(a) Photocatalytic decolorization of MO with the addition of scavengers for A2 at 20 °C; (b) schematic diagram of the possible photocatalytic mechanism*

holes of LDH will migrate to Bi_2WO_6.[44] This process is beneficial for separating the photogeneration electron-hole pairs and prolonging the lifetime of the charge carriers.[45,46] The electrons on the Bi_2WO_6 surface can react with dissolved oxygen to form superoxide radicals, owing to its more negative CB position.[20] In addition, the process of the photocatalytic reaction can generate strong oxidative species, such as •OH, H_2O_2 and O_3. The reason for this is that the potentials of the holes are much more positive than the standard redox potentials of •OH/OH^- (1.99 eV *vs* NHE), H_2O_2 (1.77 eV *vs* NHE), and O_3 (2.07 eV *vs* NHE).[35, 36] These reactive species have higher responses for the photocatalytic reaction.

CONCLUSIONS

Novel Fe_3O_4/Ni-Al-Ce LDH/Bi_2WO_6 composites were synthesized successfully via a low-temperature hydrothermal method and co-precipitation process. The photocatalytic activities of the Fe_3O_4/Ni-Al-Ce LDH/Bi_2WO_6 composites were tested using the degradation of an organic dye under visible-light illumination. The results showed that the A2 composite exhibited significantly enhanced performance in the photocatalytic reaction. In addition, after the fourth recycling run, it still maintained higher photocatalytic activity. Therefore, the Fe_3O_4/Ni-Al-Ce LDH/Bi_2WO_6 composite material is a catalyst with high activity and stability. The discovery of novel catalysts not only provides a new route for preparing heterojunction photocatalysts but also provides a possible method for the development of wastewater treatment.

REFERENCES

1. Capra, A.; Scicolone, B.; *Agric. Water Manage.* **2004**, *68*, 135.
2. Zhai, H. F.; Li, A. D.; Kong, J. Z.; *J. Solid State Chem.* **2013**, *202*, 6.
3. Yu, F.; Chang, C.; Peng, C.; *J. Hazard. Mater.* **2013**, *254-255*, 185.
4. Cui, Y. M.; Liu, L.; Zhou, X. F.; *J. Phys. Chem. C* **2010**, *114*, 2434.
5. Malekshoar, G.; Pal, K.; He, Q.; *Ind. Eng. Chem. Res.* **2014**, *53*, 18824.
6. Anzures, F. M.; Rivas, F. C.; Ventura, J. H.; *Appl. Catal., A* **2015**, *489*, 218.
7. Meng, S.; Wang, W.; Lin, Z.; *J. Hazard. Mater.* **2009**, *172*, 338.
8. Tian, G. H.; Chen, J.; Fu, H. J.; *CrystEngComm* **2014**, *16*, 842.
9. Liu, C.; Huang, H.; Du, X.; *J. Phys. Chem. C* **2015**, *119*, 17156.
10. Nguyen, D. P.; Luc, H. H.; Chen, X. B.; *J. Alloys. Compd.* **2015**, *647*, 123.
11. Anukorn, P.; Arin, M.; Phattranit, D.; *Mater. Lett.* **2015**, *159*, 289.
12. Jiang, L.; Wang, L. Z.; Zhang, J. L.; *Chem. Commun.* **2010**, *46*, 8067.
13. Zhang, M. Y.; Zhang, P.; Liu, Y.; *CrystEngComm* **2012**, *14*, 605.
14. Chen, G.; Li, F.; Huang, Z.; *Catal. Commun.* **2015**, *59*, 140.
15. Chaudhary, A.; Nag, M. P.; Ravishankar, N.; *J. Phys. Chem. C* **2014**, *118*, 29788.
16. Xu, Y. S.; Zhang, Z. J.; Zhang, W. D.; *Mater. Res. Bull.* **2013**, *48*, 1420.
17. Huang, Z.; Wu, P.; Lu, Y.; *J. Hazard. Mater.* **2013**, *246-247*, 70.
18. Wang, X. R.; Wu, P.; Lu, Y.; *Sep. Purif. Methods* **2014**, *132*, 195.
19. Seftel, E. M.; Mertens, M.; Cool, P.; *Appl. Catal., B* **2013**, *134*, 274.
20. Li, H. P.; Deng, Q. H.; Li, J. Y.; *Catal. Sci. Technol.* **2014**, *4*, 1028.
21. Seftel, E. M.; Puscasu, M. C.; Mertens, M.; *Appl. Catal., B* **2015**, *164*, 251.
22. Valente, J. S.; Tzompantzi, F.; Prince, J.; *Appl. Catal., B* **2011**, *102*, 276.
23. Leng, Y.; Zhao, J.; Jiang, P.; *ACS Appl. Mater. Interfaces* **2014**, *6*, 5947.
24. Liu, X.; Xin, L.; Yong, H.; *Talanta* **2014**, *119*, 341.
25. Wang, L.; Yu, Y.; Chen, P. C.; *J. Power Sources* **2008**, *183*, 717.
26. Xu, C. S.; Yi, F. Z.; Rong, M.; *J. Hazard. Mater.* **2011**, *192*, 186.
27. Zhang, L.; *RSC Adv.* **2015**, *5*, 30239.
28. He, Q. H.; Zhang, Z. X.; Xiong, J. W.; *Opt. Mater.* **2008**, *31*, 380.
29. Crane, M.; Frost, R. L.; Williams, P. A.; *J. Raman Spectrosc.* **2002**, *33*, 62.
30. Zhang, L.; Wang, H.; Cheng, H.; *Adv. Mater.* **2009**, *21*, 1286.
31. Ge, M.; Liu, L.; *Mater. Sci. Semicond. Process.* **2014**, *25*, 258.
32. Yu, J. C.; Yu, J. G.; Ho, W. K.; *Chem. Mater.* **2002**, *14*, 3808.
33. Chen, X. T.; Mi, F.; Zhang, H.; *Mater. Lett.* **2012**, *69*, 48.
34. Karunakaran, C.; Vinayagamoorthy, P.; Jayabharathi, J.; *Langmuir* **2014**, *30*, 15031.
35. Min, Y. L.; Zhang, F. J.; Zhao, W.; *Chem. Eng. J.* **2012**, *209*, 215.
36. Xu, M.; Han, L.; Dong, S. J.; *ACS Appl. Mater. Interfaces* **2013**, *5*, 12533.
37. Sun, L.; Qi, Y.; Jia, C. J.; *Nanoscale* **2014**, *6*, 2649.
38. Xie, T.; Xu, L.; Liu, C.; *Dalton Trans.* **2013**, *43*, 2211.
39. Jiang, Z.; Wei, W.; Mao, D.; *Nanoscale* **2014**, 7, 784.
40. Li, H.; Liu, H. J.; Hou, W.; *Key Eng. Mater.* **2014**, *160-161*, 89.
41. Gu, L. A.; Wang, J. Y.; *J. Hazard. Mater.* **2014**, *368*, 216.
42. Katsumata, H.; Sakai, T.; Suzuki, T.; *Ind. Eng. Chem. Res.* **2014**, *53*, 8018.
43. Bo, H.; Ca, F.; Chen, T.; *ACS Appl. Mater. Interfaces* **2015**, *7*, 18247.
44. Zhang, Y.; Lu, J. N.; Jin, H.; *RSC Adv.* **2015**, *5*, 48983.
45. Wang, C. C.; Hsueh, Y. C.; Su, C. Y.; *Nanotechnology* **2015**, *26*, 1535.
46. Jiang, Z. F.; Wei, W.; Xie, J. M.; *Nanoscale* **2015**, *7*, 784.